Applied Thermal Engineering 145 (2018) 264–276

Contents lists available at ScienceDirect

Applied Thermal Engineering

journal homepage: www.elsevier.com/locate/apthermeng

Research Paper

# Entropy generation minimisation of shell-and-tube heat exchanger in crude oil preheat train using firefly algorithm

Moses Omolayo Petinrin[a,b], Tunde Bello-Ochende[a,*], Ademola Adebukola Dare[b], Miracle Olanrewaju Oyewola[b]

[a] Department of Mechanical Engineering, University of Cape Town, Cape Town, South Africa
[b] Department of Mechanical Engineering, University of Ibadan, Ibadan, Nigeria

## HIGHLIGHTS

- entropy generation optimisation of typical STHE was studied.
- the optimisation model was solved using firefly algorithm.
- irreversibility distribution was largely dominated by heat transfer.
- great reduction in pumping power caused by entropy generation due to fluid friction.
- STHE with smaller heat transfer surface area and shell volume to the selected samples.

## ARTICLE INFO

*Keywords:*
Shell-and-tube heat exchanger
Preheat train
Entropy generation rate
Firefly algorithm
Pumping power

## ABSTRACT

This paper presents the entropy generation analysis and optimisation of typical shell-and-tube heat exchanger in the preheat train of crude oil distillation unit. The implication of entropy minimisation on energy consumption associated with design of heat exchanger was studied. The developed optimisation model was solved by employing the firefly algorithm. A number of constraints were applied with thirteen decision variables. The $\varepsilon$-NTU method and Delaware method were used for the heat exchanger design. Four cases were considered for each of two selected samples and were categorised under two studies. Total entropy generation rates for all the four cases considered were almost the same, and the dominant irreversibility distribution is by heat transfer. However, the sharp decrease in entropy generation due to fluid friction caused a great reduction in pumping power in the range of 51.4–82.1% and 54.8–92.2% for the two studies, respectively. The results of sensitivity study on the decision variables showed sharp reduction in entropy generation rate and increased pumping power as the mass flow rate increases for all the variables. Also, the choices of the tube diameter and tube number had greater impact on the changes in entropy generation rate and pumping power.

## 1. Introduction

Crude oil is one of the most exploited global energy resources and is refined into different forms of consumer products, such as fuels and other petrochemical products for human use. The crude oil, which is normally preheated in a network of heat exchangers, is separated into its fractions of lower hydrocarbons in refineries from the crude oil distillation unit (CDU) [1]. It is recorded that about 5–6% of the refinery fuel is consumed for refining purposes while nearly 50% of this is burnt in the CDU [2]. The largest thermal energy consumption is attributed to fractionating crude oil as compared to other processes carried out in petrochemical industries [3]. Cost-effective energy-consuming systems are required to meet up with the high demand placed on the refined products [4]. A typical preheat train for crude oil processing consists of mostly shell-and-tube heat exchangers (STHE) in series and parallel [5]. This is attributed to their robust geometry and ease of maintenance, repair and upgrade [6]. The preheat train demands efficient recovery of heat through proper optimised design of components, network and the process integration techniques [2,7].

Several types of research have been conducted on modelling of fouling characteristics and retrofitting and self-heat recuperating of the heat exchanger networks to mitigate the energy loss in the preheat train. Although, Nasr et al. [8] proposed a model for evaluating fouling in the crude oil preheat exchanger trains and were able to draw the

* Corresponding author.
*E-mail address:* tunde.bello-ochende@uct.ac.za (T. Bello-Ochende).

https://doi.org/10.1016/j.applthermaleng.2018.09.045
Received 30 April 2018; Received in revised form 23 July 2018; Accepted 8 September 2018
Available online 11 September 2018
1359-4311/ 

**Nomenclature**

*Abbreviations and symbols*

| | |
|---|---|
| $A$ | heat transfer surface area ($m^2$) |
| BC | Baffle cut (%) |
| $Be$ | Bejan number |
| $C^*$ | heat capacity ratio |
| $c_p$ | specific heat capacity (J/kg K) |
| $D_s$ | shell inside diameter (mm) |
| $d$ | tube diameter (mm) |
| G | mass velocity ($kg/m^2s$) |
| H | bulk enthalpy (J/kg) |
| $h$ | heat transfer coefficient ($W/m^2$ K) |
| $k$ | thermal conductivity (W/m K) |
| $L$ | tube length |
| $\dot{m}_s$ | mass flow rate (kg/s) |
| $N_c$ | effective number of tube rows in baffle window |
| $N_{ct}$ | total number of tubes crossed |
| $N_{cs}$ | central spacing number |
| $N_{tp}$ | number of tube passes |
| $NTU$ | number of transfer units |
| $Nu$ | Nusselt number |
| $n$ | tube number |
| $P$ | pumping power (W) |
| $Pr$ | Prandtl number |
| $PR$ | pitch ratio |
| $p_t$ | pitch (mm) |
| $q$ | heat transfer rate (W) |
| $Re$ | Reynolds number |
| $r_{BS}$ | end baffle spacing to central baffle spacing ratio |
| $r_{ss}$ | tube rows for sealing strip pair |
| $s$ | specific entropy generation rate (W/kg K) |
| $\dot{S}_g$ | entropy generation rate (W/K) |
| $T$ | temperature (K) |
| $t$ | thickness |
| $V_s$ | shell volume ($m^3$) |
| $\dot{W}$ | work transfer rate (W) |
| $\dot{X}$ | exergy lost (W) |

*Greek symbols*

| | |
|---|---|
| $\Delta p$ | pressure drop (Pa) |
| $\delta_{sb}$ | shell-to-baffle clearance |
| $\delta_{tb}$ | tube-baffle hole clearance |
| $\varepsilon$ | thermal effectiveness |
| $\eta$ | pump efficiency |
| ρ | density ($kg/m^3$) |
| $\mu$ | dynamic viscosity (Pa s) |

*Subscripts*

| | |
|---|---|
| $C$ | cold |
| $f$ | fluid friction |
| $h$ | hot |
| $h$ | heat transfer |
| $i$ | inside |
| $id$ | ideal |
| $o$ | outside |
| $in$ | inlet |
| $out$ | outlet |
| $s$ | shell |
| $t$ | tube |
| $w$ | wall |

threshold curves for fouling and no fouling formation zones. Yeap et al. [3] also used some thermo-hydraulic fouling models to carry out retrofitting and determine the most efficient one for refinery preheat train. Similar study performed by Yeap et al. [9] demonstrated the use of the models to predict the effect of fouling on the efficiency of the preheat train over time. Survey has shown that most of the studies on fouling of heat exchangers are more concentrated on refineries processing heavy crude oil [5]. Ochoa-Estopier et al. [10] applied a more accurate retrofitting model suitable for optimising crude oil heat exchanger networks. Kansha et al. [2] have also used the self-heat recuperation method, in which the process heat is recirculated in the system without adding heat to reduce the energy lost in the distillation of crude oil. However, a more suitable global optimum solution is achieved through multi-component optimisation of design variables of a single heat exchanger [11]. This guarantees the efficient use of energy and thereby reducing the cost of production of refined products [4].

Generally, the performance optimisation of a system can be carried out using two different approaches; the first is based on the first law of thermodynamics while the second method is established on both the first and second laws. The second approach focuses more on system energy utilization, thereby has become the designers choice to design a more efficient system [11,12]. It relies on the concomitant use of the principles of fluid mechanics, heat and mass transfer, and engineering thermodynamics [13,14]. Such analysis has been termed the exergy analysis, and its optimisation process is either referred as thermodynamic optimization, exergy destruction minimisation or entropy generation minimisation [14,15]. The entropy generation in a system is associated with its geometry and the thermophysical properties of the working fluids [16]. Its efficiency is significantly reduced with high rate of entropy production which destroys the useful work in the system [17]. The effectiveness of a thermal system should not only be based on improved heat transfer but minimal destruction of useful work [18,19]. Therefore, the performance of any system is reliably optimised using the entropy generation minimisation [20,21].

The entropy generation minimisation had been used by a number of researchers for the optimisation of shell-and-tube heat exchangers and some other equipment. Raja et al. [22] solved a multi-objective optimisation of shell-and-tube heat exchanger involving maximisation of effectiveness and minimisation of total cost, pressure drop and number of entropy generation units. The Pareto solutions obtained for two-objective functions optimisation of effectiveness and number of entropy generation units varied relatively with other while that of four-objective functions were not proportionally varied.. Hajabdollahi et al. [23] studied the exergetic optimisation on STHE to improve their performance. Exergy efficiency and total cost were set as objective functions and they observed that the exergy efficiency increased with the total investment cost. Also, they found out that the pressure drop and high temperature difference between heat exchanger fluids had considerable effect on exergy destruction. Rao and Saroj [24] used the entropy generation method and also considered preheating of crude oil with kerosene in one of their cases. Their work was focused more on the economic optimisation of shell-tube heat exchanger and concentration was more on the superiority of selected optimisation algorithm. Guo et al. [11] used the second law approach on STHE to generate dimensionless entropy generation number and was set as objective function with about five design variables. The design optimisation was carried out using two case studies, one for fixed heat duty and the other for fixed heat transfer area. They observed increase in the heat exchanger effectiveness with drastic reduction in pumping power at the same heat duty while at the same heat transfer area, the increase in effectiveness was said to have been accompanied with higher pumping power. The exergy destruction minimisation approach was used by

Ozcelik [25] to solve an optimization problem on STHE. The optimisation design was actually on total cost in relation to the annual capital cost and exergy cost, which is dependent on thermal and hydraulic performance of the heat exchanger. For different cases considered, they were able to obtain optimal design configurations of shell-and-tube heat exchangers.

A large number of geometrical and operating variables are handled in the design optimisation of a shell-and-tube heat exchanger, which are to be carefully selected or calculated for its optimum performance [21,23]. The optimisation problem could be resolved using a number of algorithms, depending on the optimal performance required. The conventional deterministic algorithms involve long iterative steps with many trials based on several assumptions of the mechanical and thermophysical properties to get reasonable heat exchanger ratings [24]. The iterative methods are typically disadvantaged by the complexity involved and resulting oversized equipment [25]. It also time consuming and requires much expertise [26]. In order to ensure better design of STHE with optimum performance at minimal energy cost and specific constraints, many optimisation techniques developed from research studies have been successfully applied in the design of STHE, and offer better solution than the conventional optimisation algorithms [21].

The choice of optimisation algorithm is dependent on the specific goal of research, which is in form of objective functions. Different techniques had been used by researchers for different kinds of objective functions [26]. The techniques are used in relation to carefully defined objective functions (which may be in form of efficiency, pumping power, heat transfer area, exergy loss, irreversibility, entropy generation, or cost associated with capital, running or total investment on the heat exchanger), the system constraints (in form of the tube length to shell diameter ratio, range baffle spacing ratio, maximum pressure drop), and design variables like the geometrical parameters of the heat exchanger [27,28].

Many breakthroughs have been recorded on the use of evolutionary and nature-inspired algorithms for STHE design mostly based on constructal theory or on improved rating [24,29]. A few of the successfully used algorithms for STHE designs are genetic algorithm (GA) [11,25,27,30–37], non-dominated sorting genetic algorithm (NSGA-II) [23,38], Jaya algorithm (JA) [24,39], cuckoo search algorithm (CSO) [29], gravitational search algorithm (GSA) [40], firefly algorithm (FA) [29,41], heat transfer search algorithm (HTS) [22], cohort intelligence algorithm (CIA) [42], differential evolution (DE) [43,44], Tsallis differential evolution (TDE) [44], particle swarm optimisation (PSO) [26] and imperialist competitive algorithm (ICA) [45].

Although, a lot of researches have been carried out on the optimisation of shell-and-tube heat exchangers, which are either on maximising efficiency, minimising heat transfer area, minimising pumping power, minimising exergy destruction or entropy generation, or minimising the cost (running, capital, annual and investment), none of the reviewed literatures focuses on the optimisation of shell-and-heat exchangers for crude oil refining processes. This is with the exception of few authors that took sample cases in their studies, such as Patel and Rao [26], and Rao and Saroj [24]. A large number of the literatures were on the economic optimisation design of shell-and-tube heat exchangers and the few that carried out exergetic optimisation did not explicitly examine for the dominance of the entropy generation due to heat transfer or friction and its contribution to pumping power. Placing constraint on heat transfer area or shell volume could have solved issues of conflict reported in the review literatures on multi-objective optimisation of exergy efficiency (or irreversibility reduction) and total cost. Since a lower heat transfer area will ensure a heat exchanger with a reduced capital cost [38] and also space usage can be reduced with smaller shell volume. A more realistic optimisation of a STHE requires a careful selection of the constraints (geometrical and operational) as recommended in the design codes [28,34] and the design variables (internal and external diameters of tube, tube layout, tube pitch ratio, tube number, number of tube-passes, baffle cut, inlet, outlet and central baffle spacing, tube-baffle hole clearance, shell-to-baffle clearance, tube bundle diameter, number of sealing strips, fluid allocation and so on) [46,47]. It was also observed from these literatures that only a few attempted to consider higher number of the constraints and the design variables. Such considerations are very crucial for optimised design of STHE in the crude oil preheat train, as they may negatively affect energy consumption.

Thus, this study is aimed at minimising entropy generation in typical shell-and-tube heat exchanger in the crude oil preheat train, taking into consideration the design constraints and variables as being guided by shell-and-tube heat exchanger design standards. All the earlier listed design variables will be considered as the decision variables except for the fluid allocation, in which the crude oil will be placed in the tube-side. Although certain factors must be taken into account while allocating the fluids in the sides of the heat exchanger [46,48], the choice of crude oil in the tubes-side is based on high fouling and corrosive tendency [49]. The $\varepsilon$-NTU method will be used to model the overall thermal characteristic of the STHE while the Delaware design approach will be employed to determine the shell-side heat transfer coefficient and pressure drop. The resulting optimisation model will be solved by the firefly algorithm (FA) and the sensitivity analysis of the objective function will be performed using the decision variables. It is pertinent to note from the reviewed literatures that FA has not used to optimise STHE design from exergetic point of view but only for economic reasons as seen in [29,41]. For similar cases to be considered, heat exchangers will be optimised at same heat duty but at lower or equal heat surface area and shell volume to those in samples from literature. The contributions of heat transfer and fluid friction will also be examined.

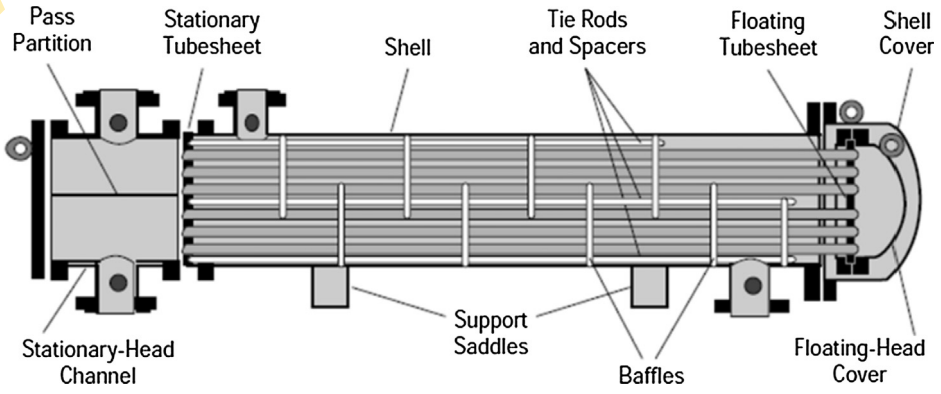


**Fig. 1.** The TEMA AES heat exchanger [58].

## 2. The firefly algorithm

Firefly algorithm is a nature-inspired metaheuristic optimization algorithm, which was developed based on the flashing and behavioural patterns of fireflies by Xin-She Yang in 2008 [50–52]. The swarm intelligence algorithm mimics the nature of how fireflies signal with their flashing light to attract mates or identify predators [53]. With this nature, the stochastic algorithm randomly searches for global optimum solutions to optimisation problems [54]. As reviewed by Fister et al. [55] the algorithm has been further classified among other metaheuristic optimization algorithms as population-based and attracted-based algorithm on the basis of the number of fireflies and their attractions together through their brightness. According to Fister et al. [54], Tilahun and Ngnotchouye [56], FA has been used in almost all the engineering disciplines ranging from wireless sensor networks, construction system reliability analysis, robotics, imaging processing, beam design, groundwater remediation, tower structures design, truss structures, antenna design, heat exchanger design and so on.

## 3. The shell-and-tube heat exchanger design formulation

The shell-and-tube heat exchanger (STHE) optimal design was carried out on an efficient and commonly used heat exchanger in the oil industry, the TEMA AES [57]. It has shell type E with split backing ring floating-head (Fig. 1) [58]. Also, the baffle selected for the purpose of this work is the single-segmental baffle, which is prominently used in STHEs for its high thermal characteristics and ease of maintenance [59].

The sensible heat transfer rate was determined either from the temperature difference on the tube-side or the shell-side of a heat exchanger as [60]

$$q = \dot{m}_t c_{p,t}(T_{t,in} - T_{t,out}) = \dot{m}_s c_{p,s}(T_{s,in} - T_{s,out}) \tag{1}$$

The effectiveness – Number of transfer units ($\varepsilon$-NTU) method was used to calculate the shell outlet temperature, which is the measure of thermal performance of a heat exchanger and it is determined from the actual sensible heat transfer rate and the maximum possible heat transfer rate of the heat exchanger [46,47]. Hence,

$$\varepsilon = \frac{q}{q_{\max}} \tag{2}$$

where

$$q_{\max} = (\dot{m}c_p)_{\min}(T_{h,in} - T_{c,in}) \tag{3}$$

and $(\dot{m}c_p)_{\min}$ is the minimum heat capacity rate of either the hot or cold fluid

Therefore, the effectiveness of one shell-pass and two-tube passes shell-and-tube heat exchanger (1–2 STHE), as obtained from [61] is determined as

$$\varepsilon = \frac{2}{(1 + C^*) + (1 + C^{*2})^{1/2}\coth\left(\frac{NTU}{2}(1 + C^*)^{1/2}\right)} \tag{4}$$

while that of one shell-pass and four-tube passes (1–4 STHE) for fluid mixed (TEMA E) when fluid with minimum heat capacity is on the tube side is estimated from

$$\varepsilon = \frac{4}{2(1 + C^*) + (1 + 4C^{*2})^{1/2}\coth\left(\frac{NTU}{4}(1 + 4C^*)^{1/2}\right) + \tanh\left(\frac{NTU}{4}\right)} \tag{5}$$

The equivalent equation for fluid with minimum heat capacity on the shell-side is

$$\varepsilon = \frac{4}{2(1 + C^*) + (1 + 4C^{*2})^{1/2}\coth\left(\frac{NTU}{4}(1 + 4C^*)^{1/2}\right) + C^*\tanh\left(\frac{C^*NTU}{4}\right)} \tag{6}$$

where the heat capacity ratio of the fluids and NTU are respectively, given as

$$C^* = \frac{(\dot{m}c_p)_{\min}}{(\dot{m}c_p)_{\max}} \tag{7}$$

and

$$NTU = \frac{UA}{(mc_p)_{\min}} = \frac{U_o A_o}{(mc_p)_{\min}} = \frac{U_i A_i}{(mc_p)_{\min}} \tag{8}$$

Given the total outer heat transfer surface area, $A_o$ from the tube outside diameter, $d_o$; length of the tubes, $L$; and the number of tubes, n in the heat exchanger as

$$A_o = \pi d_o L n \tag{9}$$

we have

$$U_o = \frac{1}{\frac{1}{h_i}\frac{d_o}{d_i} + R_{f,i}\frac{d_o}{d_i} + \frac{d_o \ln(d_o/d_i)}{2k_t} + R_{f,o} + \frac{1}{h_o}} \tag{10}$$

where $k_t$ is the thermal conductivity of the tube, $R_{f,i}$ and $R_{f,o}$ are the inside and outside fouling resistance of the tubes, $h_i$ and $h_o$ are the tube and shell-side heat transfer coefficients, respectively.

Thus, the tube inner diameter is determined from the tube outside diameter and thickness of the tube as

$$d_i = d_o - 2t_t \tag{11}$$

### 3.1. Tube-side heat transfer coefficient and pressure drop

The heat transfer coefficient on the tube-side is calculated from

$$h_i = \frac{Nu_i k_i}{d_i} \tag{12}$$

However, the tube-side Nusselt number, $Nu_i$ is determined from [61]

$$Nu_i = \begin{cases} 1.86\left[RePr\frac{d_i}{L}\right]^{1/3}\left(\frac{\mu}{\mu_w}\right)^{0.14} & Re \leqslant 2.3 \times 10^3 \\ 0.116(Re^{2/3} - 125)Pr^{1/3}\left[1 + \left(\frac{d_i}{L}\right)^{2/3}\right]\left(\frac{\mu}{\mu_w}\right)^{0.14} & 2.3 \times 10^3 \leqslant Re < 10^4 \\ 0.023Re^{0.8}Pr^{1/3}\left(\frac{\mu}{\mu_w}\right)^{0.14} & Re \geqslant 10^4 \end{cases} \tag{13}$$

The pressure drop on the tube side is estimated from [49]

$$\Delta p_t = \Delta p_f + \Delta p_r + \Delta p_{n,t} \tag{14}$$

where $\Delta p_f$, which is the pressure drop associated with fluid friction, is determined as

$$\Delta p_f = \frac{f_t N_p L G_t^2}{2000 d_i s}\left(\frac{\mu}{\mu_w}\right)^{-m} \quad \begin{cases} f_t = 64/Re & m = 0.25 \quad Re < 2300 \\ f_t = 0.4137Re^{-0.2585} & m = 0.14 \quad Re \geqslant 2300 \end{cases} \tag{15}$$

The pressure drop due to minor losses, $\Delta p_r$ is estimated from

$$\Delta p_r = 5.0 \times 10^{-4}\alpha_r G_t^2/s \tag{16}$$

Given the expression for number of velocity heads, $\alpha_r$ allocated for minor losses to be

$$\alpha_r = \begin{cases} 3.25N_p - 1.5 & Re \geqslant 2300 \\ 2N_p - 1.5 & 500 \leqslant Re < 2300 \end{cases} \tag{17}$$

And the pressure drop in the nozzles, $\Delta p_n$ is given as

$$\Delta p_{n,t} = \begin{cases} 1.5 \times 10^{-3} N_s G_{n,t}^2/sg_t & 100 \leqslant Re_{n,t} < 2300 \\ 7.5 \times 10^{-4} N_s G_{n,t}^2/sg_t & Re_{n,t} \geqslant 2300 \end{cases} \tag{18}$$

From Eqs. (15)–(18), $N_p$ is the number of tube-side passes, $N_s$ is the number of series connection of shells, $G_t$ represents the mass velocity

while $s$ is the specific gravity of fluid.

### 3.2. Shell-side heat transfer coefficient and pressure drop

The Delaware method is adopted for calculating the shell-side heat transfer coefficient and pressure drop across the shell-and-tube heat exchanger. It is has been widely used and considered to be a more accurate method in the open literature [46,47]. Although, there are many versions, the method presented here is based on modifications given by Taborek [46,62].

The shell-side heat transfer is calculated from

$$h_o = h_{o,id} J_c J_l J_b J_r J_s \tag{19}$$

where $h_{id}$ is the ideal tube bank heat transfer coefficient, $J_c$, $J_l$, $J_b$, $J_r$ and $J_s$ stand for the correction factors for baffle window flow, baffle leakage, bundle bypass, laminar flow and unequal baffle spacing, respectively.

To determine the ideal tube bank heat transfer coefficient, we have

$$h_{o,id} = j c_{p,s} G_s Pr^{-2/3} \left(\frac{\mu}{\mu_w}\right)^{0.14} \tag{20}$$

In the Eq. (20), the heat transfer factor, j was estimated from

$$j = a_1 \left(\frac{1.33}{p_t/d_o}\right)^a Re^{a_2} \tag{21}$$

and

$$a = \frac{a_3}{1 + 0.14\mathrm{Re}^{a_4}} \tag{22}$$

The constants $a_1$, $a_2$, $a_3$ and $a_4$ were looked up in a table given in [49] for each tube layout and Reynolds number regime.

Also, the maximum shell-side cross-flow mass velocity, $G_s$ is given as

$$G_s = \frac{\dot{m}_s}{S_m} \tag{23}$$

where $S_m$ is the cross-flow area and is calculated as

$$S_m = B\left[(D_s - D_{otl}) + \frac{D_{otl} - d_o}{p_{t,eff}}(p_t - d_o)\right] \tag{24}$$

The shell diameter is obtained from

$$D_s = \frac{D_{otl} + 25.44}{0.98292} \tag{25}$$

However, Eq. (26) was derived from curved-fitted equation for the clearance between the tube bundle and shell diameter for split backing ring floating-head shell-type from Taborek [62], given as

$$\delta_{sbu} = 0.01708 D_s + 25.44 \tag{26}$$

and its relationship with the outer tube limit diameter, $D_{otl}$, that is

$$\delta_{sbu} = D_s - D_{otl} \tag{27}$$

Also the expression for the outer tube limit diameter, $D_{otl}$, was adopted from [30] after careful layout sketches of various equations for tube layout to match the size of tube bundle as

$$D_{otl} = 0.637 p_t \sqrt{\pi n \left(\frac{CL}{CTP}\right)} \tag{28}$$

Here, $CL$ is the constant for tube layout, which is 1 for 45° and 90° layouts and 0.8667 for 30° layout. The $CTP$ is the constant for tube count, and for this study it is given as 0.90 and 0.77 for two-tube and four-tube passes, respectively.

The effective tube pitch diameter, $p_{t,eff}$ is

$$p_{t,eff} = \begin{cases} p_t & 30°,\ 90° \\ p_t/\sqrt{2} & 45° \end{cases} \tag{29}$$

The expressions for the correction factors for the shell-side heat transfer coefficient are:

$$J_c = 0.55 + 0.72 F_c \tag{30}$$

$$J_l = 0.44(1 - r_s) + [1 - 0.44(1 - r_s)] \exp(-2.2 r_l) \tag{31}$$

$$J_b = \begin{cases} \exp[-C_j (S_b/S_m)(1 - \sqrt[3]{2r_{ss}})] & r_{ss} < 0.5 \\ 1.0 & r_{ss} \geqslant 0.5 \end{cases} \tag{32}$$

$$J_s = \frac{(n_b - 1) + (B_{in}/B)^{(1-n_1)} + (B_{out}/B)^{(1-n_1)}}{(n_b - 1) + (B_{in}/B) + (B_{out}/B)} \tag{33}$$

and

$$J_r = \begin{cases} (10/N_{ct})^{0.18} & Re \leqslant 20 \\ 1.0 & Re \geqslant 100 \end{cases} \tag{34}$$

while $J_r$ for $20 < Re < 100$ is calculated from linear interpolation between the range given in Eq. (34) and in this study, the two end baffle spacings, $B_{in}$ and $B_{out}$ are equal.

The end baffle spacings are related to the central baffle spacing, $B$ using the following relation

$$B_{in} = r_{BS} B \tag{35}$$

Also, the central baffle spacing is determined from the tube length as

$$B = \frac{L}{2r_{BS} + N_{cs}} \tag{36}$$

where $r_{BS}$ is the ratio of the end baffle spacing to the central baffle spacing and $N_{cs}$ is the number of the central baffle spacings

The pressure drop across the shell-side as obtained from [62] is estimated as

$$\Delta p_s = \Delta p_c + \Delta p_w + \Delta p_e + \Delta p_{n,s} \tag{37}$$

The four terms in Eq. (37) are components of pressure drop in pure cross-flow at central baffle spacings, baffle windows, end zones and shell nozzles, respectively.

where each of the terms is expressed as

$$\Delta p_c = (n_b - 1) \Delta p_{id} R_l R_b \tag{38}$$

$$\Delta p_w = n_b \Delta p_{w,id} R_l \tag{39}$$

$$\Delta p_e = 2\Delta p_{id} \left(1 + \frac{N_{cw}}{N_c}\right) R_b R_s \tag{40}$$

and

$$\Delta p_{n,s} = \begin{cases} 1.5 \times 10^{-3} N_s G_{n,s}^2 / s g_s & 100 \leqslant Re_{n,s} < 2300 \\ 7.5 \times 10^{-4} N_s G_{n,s}^2 / s g_s & Re_{n,s} \geqslant 2300 \end{cases} \tag{41}$$

From these equations, the ideal pressure drop over a tube bank and the ideal pressure drop in one baffle window are given, respectively as

$$\Delta p_{id} = \frac{2 f_s N_c G^2}{\rho_s} \left(\frac{\mu}{\mu_w}\right)^{-0.14} \tag{42}$$

and

$$\Delta p_{w,id} = \begin{cases} \frac{26\mu\dot{m}_s}{\rho_s \sqrt{S_m S_w}} \left[\frac{N_{cw}}{p_t - d_o} + \frac{B}{D_w^2}\right] + \frac{\dot{m}_s^2}{\rho_s S_m S_w} & Re_s \geqslant 100 \\ \frac{(2 + 0.6 N_{cw}) \dot{m}_s^2}{2\rho_s S_m S_w} & Re_s < 100 \end{cases} \tag{43}$$

The friction factor, $f_s$ in Eq. (42) was calculated from

$$f_s = b_1 \left(\frac{1.33}{p_t/d_o}\right)^b Re^{b_2} \tag{44}$$

and

$$b = \frac{b_3}{1 + 0.14Re^{b4}} \tag{45}$$

The constants $b_1$, $b_2$, $b_3$ and $b_4$ were also obtained in a table in [49] for each tube layout and Reynolds number regime.

In order not to be repeating the whole process for the shell-and-tube heat exchanger design, the full details of other definition of terms and variables given in the above equations can be found in [49,62]

Thus, the total pumping power consumed by the heat exchanger is estimated as [11,27]

$$P = \frac{1}{\eta}\left(\frac{\dot{m}_t}{\rho_t}\Delta p_t + \frac{\dot{m}_s}{\rho_s}\Delta p_s\right) \tag{46}$$

where the pump efficiency, $\eta$ is assumed to be 80%.

### 3.3. The entropy generation minimization analysis

Based on the first and second laws of thermodynamics, the exergy balance of stream flow in a heat exchanger, which is derived from the work transfer rate $\dot{W}_{rev}$, net work transfer rate, $\dot{W}_{net}$ and the exergy lost, $\dot{X}$ can be given as [13,14]

$$\dot{W}_{rev} - \dot{W}_{net} = \dot{X}_{lost} \tag{47}$$

The work transfer rate is determined from inflow and outflow exergy of the system as

$$\dot{W}_{rev} = \dot{X}_{in} - \dot{X}_{out} \tag{48}$$

Expanding Eq. (48) for a steady energy flow, while assuming that the exergy contributions from kinetic and potential energy are negligible [63], we have

$$\dot{W}_{rev} = \left(1 - \frac{T_e}{T^*}\right)Q^* + \dot{m}\left[H_{in} - H_{out} - T_e(s_{in} - s_{out})\right] \tag{49}$$

The first term in Eq. (49) becomes zero since there is no source of heat within the heat exchanger and neither were any heat interaction with its environment. Thus for an adiabatic flow from the first law of thermodynamics, the bulk enthalpy, $H$ of the stream is constant along the stream [15]. Thus, the equation can be rewritten for single-phase flow process as

$$\dot{W}_{rev} = \dot{m}c_{p,e}(T_{in} - T_{out}) - \dot{m}T_e c_{p_e} \ln\frac{T_{out}}{T_{in}} \tag{50}$$

From Eqs. (43)–(46), the net work transfer rate, which is also the exergy due to irreversibility, is then given as

$$\dot{W}_{net} = \dot{m}c_{p,e}(T_{in} - T_{out}) - \dot{m}T_e c_{p_e} \ln\frac{T_{out}}{T_{in}} - \dot{X} \tag{51}$$

Since the exergy loss due to irreversibility is directly proportional to the entropy generated in the flow process [11,63], the last term in Eq. (51) is further expressed as

$$\dot{X} = T_e \dot{S}_g \tag{52}$$

Therefore, once the entropy generation in the system is minimized, the exergy loss is also reduced.

Irreversibility in a heat exchanger is caused by the finite temperature difference and the frictional pressure drop of the stream between its inlet and outlet [64–66]. Thus, the entropy generation rate due to the irreversibility from heat transfer and fluid friction within the heat exchanger is described as [12,67]

$$\dot{S}_g = \dot{S}_{g,h} + \dot{S}_{g,f} \tag{53}$$

The entropy generation rate caused by the heat transfer is [11]

$$\dot{S}_{g,h} = \dot{m}c_p \ln\frac{T_{out}}{T_{in}} \tag{54}$$

For the hot and cold streams,

$$\dot{S}_{g,h} = (\dot{m}c_p)_h \ln\frac{T_{h,out}}{T_{h,in}} + (\dot{m}c_p)_c \ln\frac{T_{c,out}}{T_{c,in}} \tag{55}$$

From the second law of thermodynamics, the entropy generation rate due to fluid friction or pressure drop for both the hot and cold incompressible streams is given as [15]

$$\dot{S}_{g,f} = \dot{m}_c\frac{v_c}{T_{c,in}}\Delta p_c + \dot{m}_h\frac{v_h}{T_{h,in}}\Delta p_h \tag{56}$$

Hence, the total entropy generation rate from the heat exchanger is given as

$$\dot{S}_g = (\dot{m}c_p)_h \ln\frac{T_{h,out}}{T_{h,in}} + (\dot{m}c_p)_c \ln\frac{T_{c,out}}{T_{c,in}} + \dot{m}_c\frac{v_c}{T_{c,in}}\Delta p_c + \dot{m}_h\frac{v_h}{T_{h,in}}\Delta p_h \tag{57}$$

The ratio of the thermal entropy generation rate to the total entropy generation rate within the heat exchanger is described as Bejan number, which is given as [68,69]

$$Be = \frac{\dot{S}_{g,h}}{\dot{S}_g} \tag{58}$$

This number, which is also known as the irreversibility distribution number, ranges between 0 and 1, the irreversibility due to heat transfer dominates the process as $Be$ approaches 1 while irreversibility caused by fluid friction prevails as Be approaches zero. Their contributions are the same at $Be = 0.5$ [15].

## 4. Objective function and constraints

In this study, the minimisation of entropy generation rate is taken as the objective function, as it gives better idea of the energy utilisation and reliable optimised performance of a system [12,20]. Therefore, we have

$$Min \quad f(x) = \dot{S}_g \tag{59}$$

In order to have a more realistic design of the shell-and-tube heat exchanger, a number of constraints were put into consideration and are generally group into two in this work, which are geometrical and operational constraints. The geometrical constraints are set in relation to the geometry of the heat exchanger. The constraints as obtained from [48,62] indicate that the tube length to shell-diameter ratio must be between 5 and 10, the central baffle spacing to shell diameter ratio is within 0.2 and 0.6, while the maximum unsupported span in baffle window must not be more than the addition of end baffle spacing and central baffle spacing. Thus, merging and rearranging these conditions, the geometry constraints function developed for this study are as follows

$$g_1(x) = 5 - L/D_s \leqslant 0 \tag{60}$$

$$g_2(x) = L/D_s - 10 \leqslant 0 \tag{61}$$

$$g_3(x) = 0.4 - (B + B_{in})/D_s \leqslant 0 \tag{62}$$

$$g_4(x) = (B + B_{in})/D_s - 1.2 \leqslant 0 \tag{63}$$

The operational constraints are working conditions of the heat exchanger. The recommended values as given by Sinnott [48] and Mukherjee [58] for the maximum velocities are 2 m/s and 1 m/s for the tube- and shell-sides, respectively. The corresponding maximum permissible pressure drops are 70 KN/m$^2$ and 35 KN/m$^2$. Therefore, the operational constraints are written as

$$g_5(x) = u_t - u_{t,\max} \leqslant 0 \tag{64}$$

$$g_6(x) = u_s - u_{s,\max} \leqslant 0 \tag{65}$$

$$g_7(x) = \Delta p_t - \Delta p_{t,\max} \leqslant 0 \tag{66}$$

$$g_8(x) = \Delta p_s - \Delta p_{s,\max} \leqslant 0 \tag{67}$$

Other constraints for specific cases were consecutively added by setting heat transfer area and shell volume of the samples from literature as critical values. As applied to each case, the added constraint is

$$g_9(x) = A_o - A_{o,critical} \leqslant 0 \tag{68}$$

or

$$g_9(x) = V_s - V_{s,critical} \leqslant 0 \tag{69}$$

Adding the constraints into the objective function using the penalty method [50]. Eq. (59) is rewritten as

$$Min \quad f(x) = \dot{S}_g + c\sum_{i-1}^{N} I_i(g_i(x))g_i^2(x) \tag{70}$$

where the penalty constant, $c = 10^{15}$, $N$ is the number of constraints and the index function $I_i(g_i(x))$ is 0 and 1 within and outside each constraint, respectively.

As presented in Table 1, a number of decision variables, containing 9 discrete and 4 continuous, were carefully selected for realistic design of heat exchanger with minimised the entropy generation rate suitable for crude oil preheat train. The choice of the variables was as guided by the heat exchanger design codes[48,49,62]. The tube diameter and thickness were selected for heat exchanger tubes ranging from BWG 10 to 18 [62,70].

## 5. Implementation of firefly algorithm

The light intensity of each firefly was taken as the entropy generation rate obtained from the random selection of multiple of decision variables. Population size of 150 fireflies was considered for a maximum number of 50 generations, which is the maximum number of iterations. The fireflies are ranked in each loop and the firefly with the minimum entropy generation rate has the highest light intensity. The less bright fireflies within the same generation are subsequently attracted to the brighter or more attractive ones to generate newer population of swarm of fireflies with the brighter firefly. This is repeated until the maximum generation is attained [50,56,71].

The attractiveness of a brighter firefly in relation to another firefly at a distance, $r$ is given by

$$\beta = \beta_0 e^{-\gamma r^2} \tag{71}$$

The Cartesian distance between two fireflies $i$ and $j$ at positions $x_i$ and $x_j$, is given as

$$r_{ij} = ||x_i - x_j|| = \sqrt{\sum_{k=1}^{d}(x_{i,k} - x_{j,k})^2} \tag{72}$$

In Eq. (72), the positions $x_i$ and $x_j$ are two parameters in the range of any of the decision variables and $d$ is the dimension of the decision variables, which are 13.

Thus, a firefly $i$ is moved towards a more attractive firefly $j$ by changing the position $x_i$ of any component $k$ using

$$x_i = x_i + ((\beta_0 - 0.2)e^{-\gamma r_{ij}^2} + 0.2)(x_j - x_i) + \alpha(r_d - 0.5) \tag{73}$$

The movement for the discrete variables was determined from

$$x_i = round(x_i + ((\beta_0 - 0.2)e^{-\gamma r_{ij}^2} + 0.2)(x_j - x_i)) \tag{74}$$

However, before determining the new position, $x_i$ for each of the 9 components of the discrete variables, all parameters within each component were assigned integer values; value of 1 was allocated to the smallest parameter and maximum dimension of the component to the highest parameter. After the movement, the new $x_i$ values were reallocated back to corresponding parameters within the component.

From Eqs. (71)–(74), $\beta_0$ represents the attractiveness at $r = 0$, $\gamma$ is a fixed light absorption coefficient, $\alpha$ is the randomisation parameter and $r_d$ is a random number between 0 and 1. Based on the practical range of values in Yang [50], $\beta_0 = 1.0$, $\gamma = 1.0$ and the initial randomization parameter, $\alpha_0 = 0.5$.

The convergence of the solution was increased by reducing the randomness parameter at every generation from its initial value using this expression:

$$\alpha_i = \alpha_{i-1}\theta^{(1/NG)} \quad i = 1, 2, 3, ....NG \tag{75}$$

where $NG$ the maximum number of generation and $\theta$ is the randomness reduction constant, which was taken as $10^{-4}/0.9$.

## 6. Structure of the optimisation process

The entropy generation optimisation model for shell-and-tube heat exchanger was solved using the procedure for firefly algorithm and was written in MATLAB code. The flowchart for the programming procedure is as depicted in Fig. 2. In this work, the effect of nozzle pressure drop and the viscosity correction factor on the tube- and shell-sides were considered to be negligible.

As indicated in Table 2, the design specifications of shell-and-tube heat exchangers were obtained as samples from literature; the first (Sample 1) was selected from Serth and Lestina [49], while the second (Sample 2) was taken from Sinnott [48]. Some design variables ($r_{ss}$, $N_{cs}$, $r_{BS}$, $\delta_{sb}$, and $\delta_{tb}$) were adopted from sample 1 to complement the variables in Sample 2, because the Kern method used for Sample 2 does not account for these variables [48]. The heat exchanger was optimised at the same heat duty with each sample, and the heat transfer surface area and shell volume were set as critical values. Thus, the optimisation process was categorised into two studies and each was subjected to the following cases:

Case 1: heat transfer surface area not more than the critical value.
Case 2: shell volume not more than the critical value.
Case 3: heat transfer surface area not more than the critical value with unknown shell outlet temperature.
Case 4: shell volume not more than the critical value with unknown shell outlet temperature.

## 7. Results and discussion

### 7.1. Model validation

In order to validate the MATLAB code, the preliminary outputs and its corresponding values for the same input data from Serth and Lestina [49] (Sample 1) were compared and are presented in Table 3. It can be seen that the differences in the corresponding output data are within acceptable limits; therefore, the developed code was used with all

**Table 1**
The range of parameters for the decision variables of the shell-and-tube heat exchanger.

| Decision variables | Range | Increment |
|---|---|---|
| Tube outside diameter, $d_o$ (mm) | 19.050, 22.225, 25.4 and 28.575 | – |
| Tube thickness, $t_t$ (mm) | 1.245, 1.651, 1.829, 2.108, 2.413, 2.769, 3.048 and 3.403 | – |
| Tube layout | 30°, 45°, and 90° | – |
| Pitch ratio, $PR$ | 1.25–2.00 | 0.05 |
| Number of tubes, $n$ | 50–550 | 1 |
| Number of tube passes, $N_{tp}$ | 2 and 4 | – |
| Tube rows for sealing strip pair, $r_{ss}$ | 4–10 | 1 |
| Baffle cut, $BC$ | 15–35° | 1 |
| Central spacing number, $N_{cs}$ | 30–70 | 1 |
| Tube Length, $L$ (mm) | 3000–8000 | – |
| End baffle to central baffle spacing ratio, $r_{BS}$ | 1.0–1.3 | – |
| Shell-to-baffle clearance, $\delta_{sb}$ | $0.005D_s$ -$0.01D_s$ | – |
| Tube-baffle hole clearance, $\delta_{tb}$ | $0.01d_o$ -$0.04d_o$ | – |

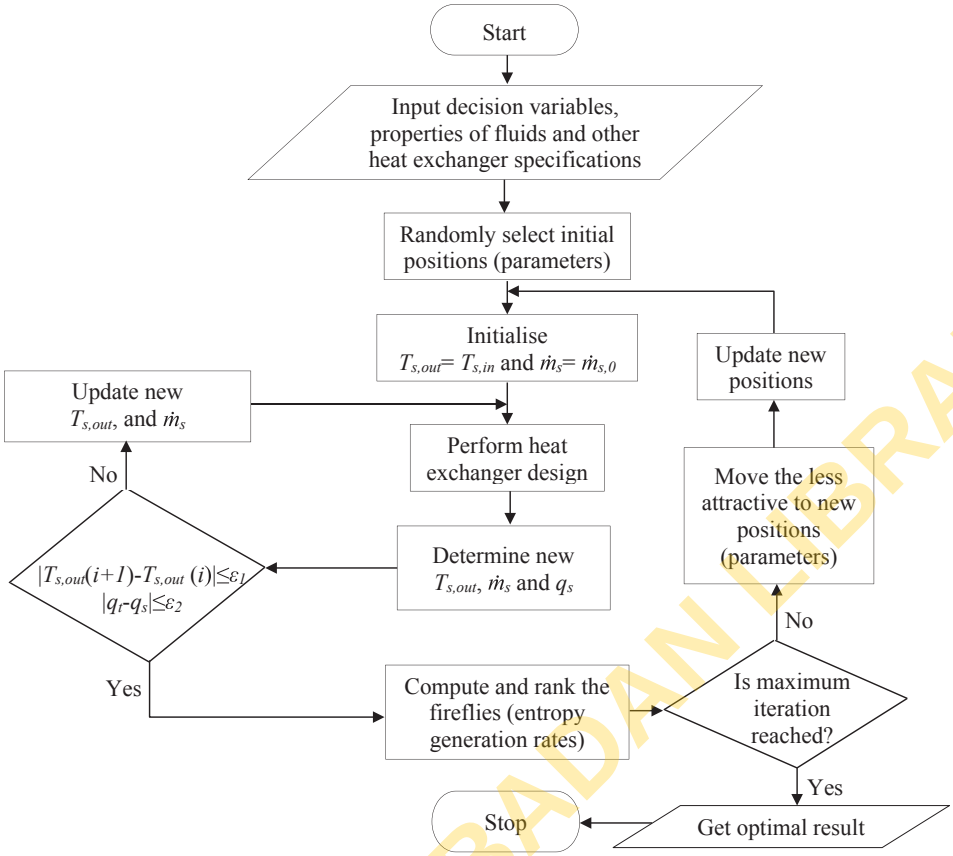


**Fig. 2.** The flowchart of the optimisation of shell-and-tube heat exchanger (Cases 3 and 4).

**Table 2**
The thermophysical properties of shell-and-tube heat exchanger.

| Process parameters | Sample 1 | | Sample 2 | |
|---|---|---|---|---|
| | Tube-side Crude Oil (32° API) | Shell-side Kerosene (48° API) | Tube-side Crude Oil (34° API) | Shell-side Kerosene (42° API) |
| Flow rate (kg/s) | 18.90 | 5.67 | 19.44 | 5.56 |
| Inlet temperature (°C) | 37.8 | 198.9 | 40.0 | 200.0 |
| Outlet temperature (°C) | 65.9 | 121.1 | 78.0 | 90.0 |
| Density (kg/m$^3$) | 849.1 | 784.2 | 820.0 | 730.0 |
| Thermal conductivity (W/m K) | 0.1333 | 0.1367 | 0.1340 | 0.1320 |
| Specific heat capacity (J/kg K) | 2051.5 | 2470.2 | 2050.0 | 2470.0 |
| Viscosity (Pa s) | 0.00359 | 0.00040 | 0.00320 | 0.00043 |
| Fouling resistance (m$^2$ K/W) | 0.00053 | 0.00035 | 0.00035 | 0.00020 |
| Thermal conductivity of tube, plain carbon steel (W/m K) | 45.006 | | 45 | |
| Heat duty (kW) | 1089.5 | | 1509.4 | |

confidence for the heat exchanger optimisation.

### 7.2. Optimisation results

The optimal design parameters from the pool of the decision variables for each of the cases are as tabulated against the each of the samples in Tables 4 and 5. Also, their corresponding optimum heat exchanger characteristics are as shown in Tables 6 and 7. It can be observed from the two studies that the reductions in entropy generation rates as compared with the samples are very small. Moreover, the irreversibility distribution is dominated by heat transfer. There were comparatively little changes in the heat transfer entropy generation rates as against entropy generation rates due to fluid friction. This indicates that the geometrical design variables contributes more to the fluid friction entropy generation rates. The reductions in entropy generation due to fluid friction are in the range of 51.4–82.1% for Study 1 and 54.8–92.2% for Study 2. Whereas, the corresponding ranges observed for the heat transfer entropy generation rate are 0.0–1.5% and 0.0–3.4%. The heat transfer entropy generation rates for Cases 1 and 2 were the same as the values obtained for samples. This can actually be ascribed to the constant stream temperatures and mass flow rates for the first two cases.

However, the very little reduction observed in the entropy generation rate from the optimisation process has significant effect on the on the pumping power. As it can be seen from Tables 6 and 7, the reductions in pumping power are in the range of 51.2–81.1% for Study 1 and 50.5–92.1% for Study 2. This would by implication reduce the pumping or running costs of the heat exchangers at the same rates. Therefore, the total investment will be greatly reduced with the reduction in the capital cost associated with the heat transfer surface area and shell volume. Further observation of the characteristics of the heat exchangers in Tables 6 and 7 shows that those cases (Cases 2 and 4) subjected to critical shell volume produced heat exchangers with reduced heat transfer surface area than their corresponding cases (Cases 1 and 3). Thus by implication capital cost of a shell-and-tube heat exchanger could be much reduced by designing for smaller shell volume

**Table 3**
The validation results.

| Output Data | Ref. [49] | Present Study | Difference (%) |
|---|---|---|---|
| $A_o$ | 42.18 | 42.22 | 0.095 |
| $\Delta p_t$ (Pa) | 65431.25 | 65424.13 | 0.011 |
| $\Delta p_s$ (Pa) | 7653.18 | 7532.29 | 1.580 |
| $h_i$ (W/m$^2$K) | 885.77 | 888.00 | −0.252 |
| $h_o$ (W/m$^2$K) | 889.17 | 889.89 | −0.081 |

**Table 4**
The optimal design parameters (Study 1).

| Study 1 | $d_o$ (mm) | $t_t$ (mm) | Layout (°) | $PR$ | $n$ | $N_{tp}$ | $r_{ss}$ | $BC$ (%) | $N_{cs}$ | $L$ (mm) | $r_{BS}$ | $\delta_{sb}$ $(1/D_s)$ | $\delta_{tb}$ $(1/d_o)$ |
|---|---|---|---|---|---|---|---|---|---|---|---|---|---|
| Sample 1 | 25.40 | 2.108 | 90 | 1.25 | 124 | 4 | 10 | 20 | 41 | 4267 | 1.0000 | 0.00517 | 0.01575 |
| Case 1 | 25.40 | 2.108 | 45 | 1.60 | 108 | 2 | 8 | 27 | 42 | 4520 | 1.1033 | 0.00755 | 0.02562 |
| Case 2 | 25.40 | 1.829 | 30 | 1.40 | 105 | 2 | 5 | 21 | 50 | 4007 | 1.2921 | 0.01000 | 0.03389 |
| Case 3 | 25.40 | 2.108 | 45 | 1.60 | 112 | 2 | 8 | 20 | 38 | 4060 | 1.2128 | 0.01000 | 0.04000 |
| Case 4 | 22.23 | 1.829 | 45 | 1.75 | 90 | 2 | 10 | 19 | 31 | 4537 | 1.2960 | 0.01000 | 0.01000 |

**Table 5**
The optimal design parameters (Study 2).

| Study 2 | $d_o$ (mm) | $t_t$ (mm) | Layout (°) | $PR$ | $n$ | $N_{tp}$ | $r_{ss}$ | $BC$ (%) | $N_{cs}$ | $L$ (mm) | $r_{BS}$ | $\delta_{sb}$ $(1/D_s)$ | $\delta_{tb}$ $(1/d_o)$ |
|---|---|---|---|---|---|---|---|---|---|---|---|---|---|
| Sample 2 | 25.40 | 2.110 | 30 | 1.25 | 360 | 4 | 10 | 25 | 41 | 5000 | 1.0000 | 0.00517 | 0.01575 |
| Case 1 | 25.40 | 1.829 | 45 | 1.60 | 194 | 2 | 7 | 25 | 39 | 5440 | 1.2471 | 0.01000 | 0.04000 |
| Case 2 | 22.23 | 2.108 | 30 | 1.30 | 217 | 2 | 10 | 32 | 35 | 4061 | 1.2594 | 0.01000 | 0.01000 |
| Case 3 | 28.58 | 3.048 | 45 | 1.90 | 115 | 2 | 8 | 32 | 31 | 5824 | 1.3000 | 0.01000 | 0.01000 |
| Case 4 | 22.23 | 1.829 | 45 | 1.70 | 111 | 2 | 10 | 20 | 31 | 4519 | 1.2896 | 0.00686 | 0.01482 |

**Table 6**
The optimum heat exchanger characteristics (Study 1).

| Study 1 | $\dot{m}_s$ (kg/s) | $T_{s,out}$ (°C) | $A_o$ (m$^2$) | $V_s$ (m$^3$) | $\Delta p_t$ (Pa) | $\Delta p_s$ (Pa) | $P$ (W) | $\varepsilon$ | $\dot{S}_{gen,f}$ (W/K) | $\dot{S}_{gen,h}$ (W/K) | $Be$ | $\dot{S}_{gen}$ (W/K) |
|---|---|---|---|---|---|---|---|---|---|---|---|---|
| Sample 1 | 5.67 | 121.1 | 42.22 | 0.8004 | 65,424 | 7532 | 1888 | 0.483 | 4.7987 | 5878 | 0.9992 | 5882 |
| Case 1 | 5.67 | 121.1 | 38.95 | 1.0247 | 12,325 | 2305 | 364 | 0.483 | 0.9176 | 5878 | 0.9998 | 5879 |
| Case 2 | 5.67 | 121.1 | 33.58 | 0.5996 | 10,334 | 7647 | 357 | 0.483 | 0.8569 | 5878 | 0.9999 | 5879 |
| Case 3 | 9.34 | 151.6 | 36.28 | 0.9528 | 10,517 | 5366 | 372 | 0.293 | 0.8882 | 5789 | 0.9998 | 5790 |
| Case 4 | 7.77 | 142.1 | 28.51 | 0.7961 | 31,562 | 3377 | 920 | 0.353 | 2.3302 | 5816 | 0.9996 | 5819 |

**Table 7**
The optimum heat exchanger characteristics (Study 2).

| Study 2 | $\dot{m}_s$ (kg/s) | $T_{s,out}$ (°C) | $A_o$ (m$^2$) | $V_s$ (m$^3$) | $\Delta p_t$ (Pa) | $\Delta p_s$ (Pa) | $P$ (W) | $\varepsilon$ | $\dot{S}_{gen,f}$ (W/K) | $\dot{S}_{gen,h}$ (W/K) | $Be$ | $\dot{S}_{gen}$ (W/K) |
|---|---|---|---|---|---|---|---|---|---|---|---|---|
| Sample 2 | 5.56 | 90.0 | 107.73 | 1.3041 | 62,802 | 72,270 | 1930 | 0.688 | 4.8718 | 8196 | 0.9994 | 8201 |
| Case 1 | 5.56 | 90.0 | 84.22 | 2.1615 | 4850 | 845 | 152 | 0.688 | 0.3808 | 8196 | 0.9999 | 8197 |
| Case 2 | 5.56 | 90.0 | 61.53 | 0.8149 | 7364 | 3773 | 254 | 0.688 | 0.6183 | 8196 | 0.9999 | 8197 |
| Case 3 | 10.68 | 145.3 | 60.12 | 2.4430 | 11,116 | 980 | 348 | 0.342 | 0.8729 | 7967 | 0.9999 | 7968 |
| Case 4 | 13.49 | 157.1 | 35.02 | 0.9154 | 23,002 | 11,421 | 955 | 0.268 | 2.2035 | 7921 | 0.9997 | 7923 |

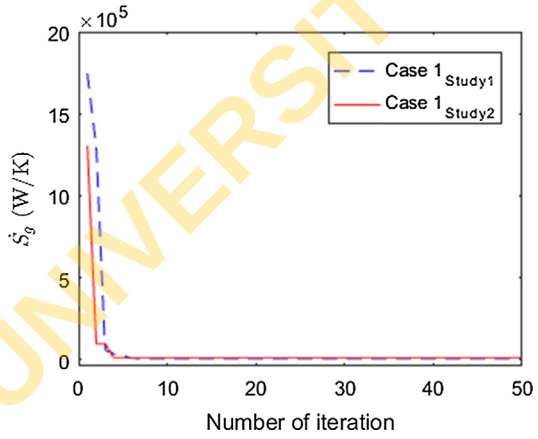


**Fig. 3.** The convergence plot of firefly algorithm.

than smaller heat transfer surface area. This as most often be attributed to the heat transfer surface area [38]. As it could also been seen from the results, more useful energy is lost due to the higher irreversibility by heat transfer with increase in thermal efficiencies. This justifies the reason for system effective modelling using the second law approach [15].

The plot of convergence of the entropy generation rate for Case 1 in each study versus the number of iterations is as shown Fig. 3. It was found that the optimisation model converges to solution within the third and fifth iteration, this can be attributed to the effectiveness of firefly algorithm at solving engineering problems [54,56].

### 7.3. Sensitivity study on the decision variables

The sensitivity of the entropy generation rate and the pumping power to the mass flow rate on the shell-side for the decision variables were observed. For each sensitivity study, the mass flow rate was varied from 2 kg/s to 14 kg/s. The study was carried out at the same heat duty using only the design specifications for Sample 1. The graph plots of results for all the decision variables are stacked into two for the convenience of presentation and are as depicted in Figs. 4 and 5. In these figures, the first four legend descriptions are for the entropy generation rate while the last four descriptions stand for the pumping power. Similar trends were observed for increase in mass flow rate, the entropy generation rate decreases appreciably and the reduction decreases as the flow rate increases. The clear variation must have been a major contribution from the changes in heat transfer entropy generation rate which is also dependent on the changing flow rate and shell-side outlet temperature at the same heat duty. Also, there was rise in pumping power with the increase in flow rate.

In Fig. 4a, the entropy generated reduces with increase in the tube diameter for the same flow rate. Although the observed difference in entropy generation rate is small, its influence on the pumping power can be seen as it increases tremendously with decrease in tube

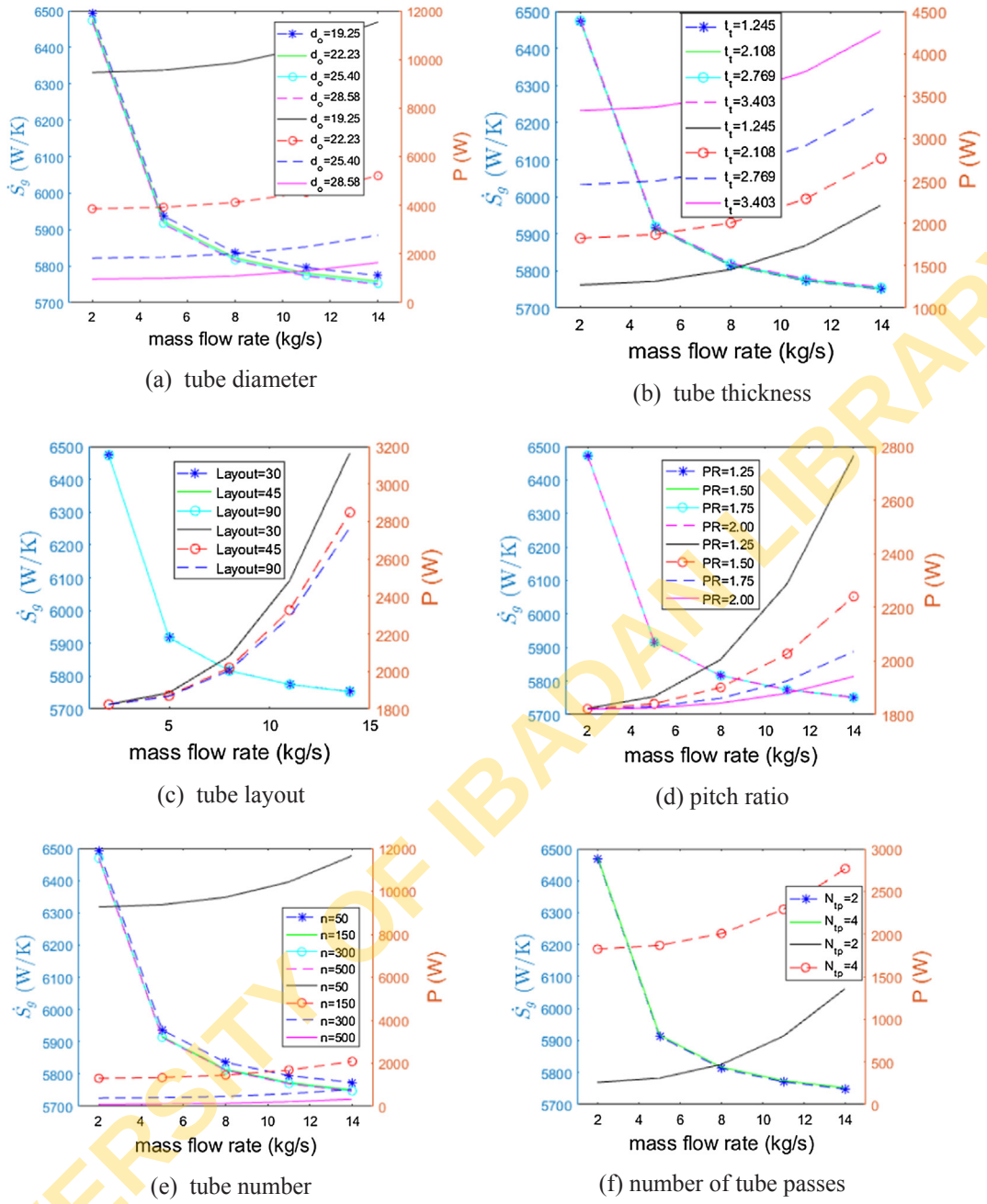


(a) tube diameter (b) tube thickness

(c) tube layout (d) pitch ratio

(e) tube number (f) number of tube passes

**Fig. 4.** The sensitivity of entropy generation rate and pumping power on the choice of decision variables.

diameter. There is very little difference in entropy generated at the same mass flow rate as the tube thickness varies in Fig. 4b. The pumping power increases with increase in tube thickness, however, the effect of change in thickness on pumping power was not as pronounced as that of tube diameter. Similar trends as the effect of the tube thickness were observed for the tube layout and pitch ratio in Fig. 4c and d. But the pumping power increases with decrease in tube layout and pitch ratio for the same mass flow rate.

Fig. 4e shows the contribution of change in tube number to the entropy generation rate and this could be seen to have serious effect on the pumping power in similar way to the tube diameter. The lower tube number generates more entropy and demands higher pumping power than the higher tube number. Although keeping all other variables constant, smaller tube number may produce smaller heat exchanger but the present result shows higher pumping power from smaller tube number. From Figs. 4f and 5a–g, the changes in entropy generation rates from the variations of the decision variables at the same mass flow rate could not be seen from the figures and appear to be insignificant. However, the changes in the pumping power could be attributed to the small changes in the entropy generation rate due to fluid friction. The effects of variation of these variables on pumping power are significantly less pronounced than those of tube diameter and tuber number. In this category, the pumping power seems to be more sensitive on the choice of central baffle spacing number and increases rapidly with the mass flow rate (Fig. 5c) while the selections of tube row per sealing strip (Fig. 5a) and end baffle to central baffle spacing ratio (Fig. 5e) do not have significant effect on the pumping power except for the quick rise in pumping power as the flow rate increases. As clearly indicated in these figures, the pumping power increases with increase in tube passes (Fig. 4f), number central baffle spacing (Fig. 5c) and tube length (Fig. 5d). Increase in pumping power could also be seeing from decrease in baffle cut (Fig. 5b), tube row per sealing strip (Fig. 5a), end baffle to central baffle spacing ratio (Fig. 5e), shell-to-baffle clearance (Fig. 5f) and tube-baffle hole clearance (Fig. 5g).

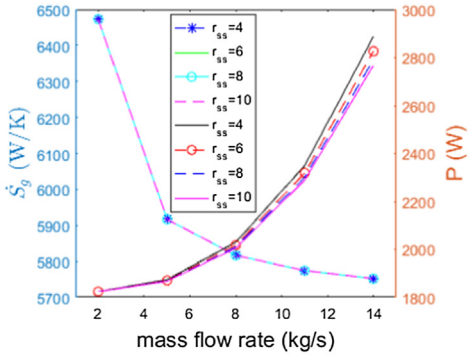


(a) tube row per sealing strip

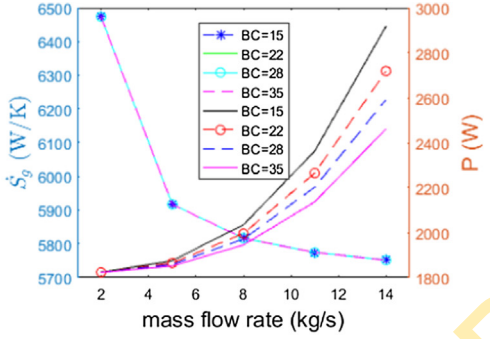


(b) baffle cut

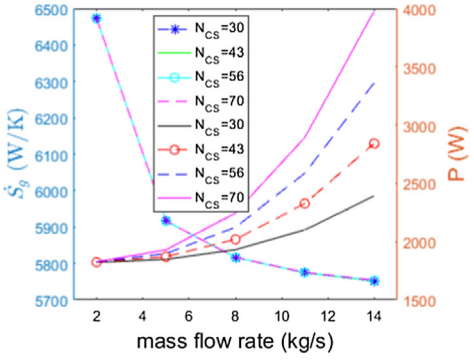


(c) number central baffle spacing

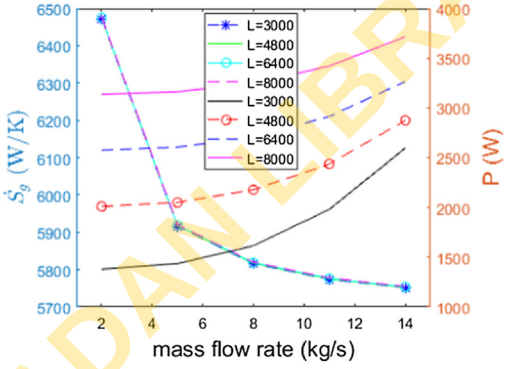


(d) tube length

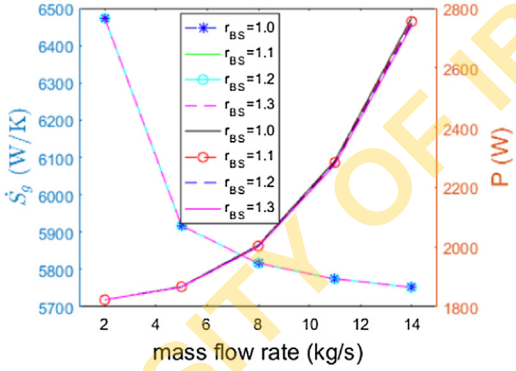


(e) end baffle to central baffle spacing ratio

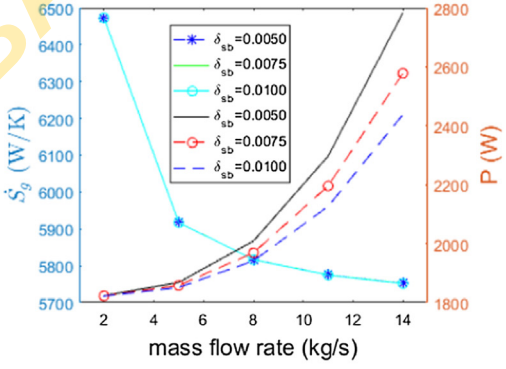


(f) shell-to-baffle clearance

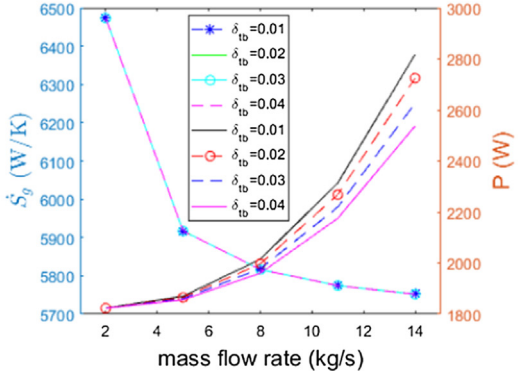


(g) tube-baffle hole clearance

**Fig. 5.** The sensitivity of entropy generation rate and pumping power on the choice of decision variables.

## 8. Conclusion

The entropy generation optimisation of typical shell-and-tube heat exchanger the crude oil preheat train has been carried out. Fourteen decision variables and a number of design constraints were selected. The developed optimisation model was successfully solved using the firefly algorithm. Two samples were selected and each with four cases which were subsequently categorised into two studies. The obtained results from the two studies showed very small reductions in the total entropy generation rates for each of the cases as compared with their respective samples. The irreversibility distribution of the heat exchangers was dominated by heat transfer and has a relatively small reduction in entropy generation as compared with the contribution of fluid friction to entropy generation. However, the sharp decrease in the entropy generation rates due to fluid friction caused significant reduction of the pumping power, and this would invariably cut down the running costs of the heat exchangers. Thus, careful and detailed optimised design of each heat exchanger in the preheat train will result into more efficient crude oil distillation unit in terms of energy consumption and running costs. Moreover, the smaller heat transfer surface area and shell volume recorded will definitely lower the capital cost, and by implication the total investment cost of the preheat train will be much reduced. As it was observed in this research work, the shell volume of a shell-and-tube heat exchanger could be better minimised than its heat transfer surface area, a smaller volume will take care of occupied space and the capital investment cost. In the sensitivity analysis study, the increase in mass flow rate of the shell-side fluid had great influence on the reduction of the total entropy generation rate but at also higher pumping power. Among the decision variables, the tube diameter and tube number showed higher sensitiveness to the entropy generation rate and pumping power while the tube row per sealing strip and end baffle spacing to central baffle spacing ratio showed less sensitivity, though the change in mass flow rate has greater influence on them. The study has presented a cost-effective and less-energy consuming model for designing shell-and-tube heat exchangers for crude oil pre-heat train. It has also open the research further for search of algorithms that may be better suited for less energy consuming heat exchangers in preheat train for than the firefly algorithm.

## Acknowledgement

The financial support of the Tertiary Education Trust Fund (TETFund), Nigeria is hereby acknowledged and duly appreciated. The authors also appreciate the use of facilities at the Department of Mechanical Engineering, University of Cape Town, South Africa.

## References

[1] S. Emani, M. Ramasamy, K. Zilati, K. Shaari, Effect of shear stress on crude oil fouling in a heat exchanger tube through CFD simulations, Proc. Eng. 148 (2016) 1058–1065, https://doi.org/10.1016/j.proeng.2016.06.592.
[2] Y. Kansha, A. Kishimoto, A. Tsutsumi, Application of the self-heat recuperation technology to crude oil distillation, Appl. Therm. Eng. 43 (2012) 153–157, https://doi.org/10.1016/j.applthermaleng.2011.10.022.
[3] B.L. Yeap, D.I. Wilson, G.T. Polley, S.J. Pugh, Mitigation of crude oil refinery heat exchanger fouling through retrofits based on thermo-hydraulic fouling models, Inst. Chem. Eng. 82 (2004) 53–71.
[4] M. Mehdizadeh-Fard, F. Pourfayaz, A.B. Kasaeian, M. Mehrpooya, A practical approach to heat exchanger network design in a complex natural gas refinery, J. Nat. Gas Sci. Eng. (2017), https://doi.org/10.1016/j.jngse.2017.02.001.
[5] M.R. Mozdianfard, E. Behranvand, Fouling at post desalter and pre fl ash drum heat exchangers of CDU preheat train Loss on Ignition, Appl. Therm. Eng. 89 (2015) 783–794, https://doi.org/10.1016/j.applthermaleng.2015.06.045.
[6] Q. Wang, G. Chen, Q. Chen, M. Zeng, Review of improvements on shell-and-tube heat exchangers with helical baffles, Heat Transf. Eng. 31 (2010) 836–853, https://doi.org/10.1080/01457630903547602.
[7] J. Khorshidi, E. Zare, A.R. Khademi, Analysis of heat exchanger network of distillation unit of shiraz oil refinery, World Acad. Sci. Eng. Technol. 10 (2016) 1269–1276.
[8] G.T. Polley, A.M. Fuentes, S.J. Pugh, Design of shell-and-tube heat exchangers to achieve a specified operating period in refinery pre-heat trains, in: H. Müller-Steinhagen, M.R. Malayeri, A.P. Watkinson (Eds.), Proc. Int. Conf. Heat Exch. Fouling Clean. VIII, Schladming, 2009, pp. 346–351.
[9] B.L. Yeap, G.T. Polley, S.J. Pugh, D.I. Wilson, Retrofitting crude oil refinery heat exchanger networks to minimize fouling while maximizing heat recovery, Heat Transf. Eng. 26 (2006) 23–34, https://doi.org/10.1080/01457630590890139.
[10] L.M. Ochoa-estopier, M. Jobson, L. Chen, Area-based optimization approach for refinery heat exchanger networks, Appl. Therm. Eng. 129 (2018) 606–617, https://doi.org/10.1016/j.applthermaleng.2017.10.049.
[11] J. Guo, L. Cheng, M. Xu, Optimization design of shell-and-tube heat exchanger by entropy generation minimization and genetic algorithm, Appl. Therm. Eng. 29 (2009) 2954–2960, https://doi.org/10.1016/j.applthermaleng.2009.03.011.
[12] A. Mwesigye, T. Bello-ochende, J.P. Meyer, Minimum entropy generation due to heat transfer and fluid friction in a parabolic trough receiver with non-uniform heat flux at different rim angles and concentration ratios, Energy 73 (2014) 606–617, https://doi.org/10.1016/j.energy.2014.06.063.
[13] A. Bejan, The method of entropy generation minimization, in: A. Bejan (Ed.), Energy Environ., Academic Publishers, 1999, pp. 11–22.
[14] A. Bejan, Fundamentals of exergy analysis, entropy generation minimization, and the generation of # ow architecture, Int. J. Energy Res. 565 (2002) 545–565, https://doi.org/10.1002/er.804.
[15] A. Bejan, Advanced Engineering Thermodynamics, fourth ed., John Wiley & Sons, Hoboken, 2016.
[16] J.A. Esfahani, M. Akbarzadeh, S. Rashidi, M.A. Rosen, R. Ellahi, Influences of wavy wall and nanoparticles on entropy generation over heat exchanger plat, Int. J. Heat Mass Transf. 109 (2017) 1162–1171, https://doi.org/10.1016/j.ijheatmasstransfer.2017.03.006.
[17] M. Bahiraei, R. Rahmani, A. Yaghoobi, E. Khodabandeh, R. Mashayekhi, M. Amani, Recent research contributions concerning use of nanofluids in heat exchangers: a critical review, Appl. Therm. Eng. 133 (2018) 137–159, https://doi.org/10.1016/j.applthermaleng.2018.01.041.
[18] M. Bahiraei, M. Jamshidmofid, S. Heshmatian, Entropy generation in a heat exchanger working with a biological nanofluid considering heterogeneous particle distribution, Adv. Powder Technol. (2017), https://doi.org/10.1016/j.apt.2017.06.021.
[19] M. Bahiraei, S. Heshmatian, Optimizing energy efficiency of a specific liquid block operated with nanofluids for utilization in electronics cooling: a decision-making based approach, Energy Convers. Manage. 154 (2017) 180–190, https://doi.org/10.1016/j.enconman.2017.10.055.
[20] M. Farzaneh-Gord, H. Ameri, A. Arabkoohsar, Tube-in-tube helical heat exchangers performance optimization by entropy generation minimization approach, Appl. Therm. Eng. (2016), https://doi.org/10.1016/j.applthermaleng.2016.08.028.
[21] M. Bahiraei, R. Khosravi, S. Heshmatian, Assessment and optimization of hydrothermal characteristics for a non-Newtonian nanofluid flow within miniaturized concentric-tube heat exchanger considering designer's viewpoint, Appl. Therm. Eng. 123 (2017) 266–276, https://doi.org/10.1016/j.applthermaleng.2017.05.090.
[22] B.D. Raja, R.L. Jhala, V. Patel, Many-objective optimization of shell and tube heat exchanger, Therm. Sci. Eng. Prog. 2 (2017) 87–101, https://doi.org/10.1016/j.tsep.2017.05.003.
[23] H. Hajabdollahi, P. Ahmadi, I. Dincer, Exergetic optimization of shell-and-tube heat exchangers using NSGA-II, Heat Transf. Eng. 33 (2012) 618–628, https://doi.org/10.1080/01457632.2012.630266.
[24] R.V. Rao, A. Saroj, Constrained economic optimization of shell-and-tube heat exchangers using elitist-Jaya algorithm, Energy 128 (2017) 785–800, https://doi.org/10.1016/j.energy.2017.04.059.
[25] Y. Ozcelik, Exergetic optimization of shell and tube heat exchangers using a genetic based algorithm, Appl. Therm. Eng. 27 (2007) 1849–1856, https://doi.org/10.1016/j.applthermaleng.2007.01.007.
[26] V.K. Patel, R.V. Rao, Design optimization of shell-and-tube heat exchanger using particle swarm optimization technique, Appl. Therm. Eng. 30 (2010) 1417–1425, https://doi.org/10.1016/j.applthermaleng.2010.03.001.
[27] A.C. Caputo, P.M. Pelagagge, P. Salini, Heat exchanger design based on economic optimisation, Appl. Therm. Eng. 28 (2008) 1151–1159, https://doi.org/10.1016/j.applthermaleng.2007.08.010.
[28] A.L.H. Costa, E.M. Queiroz, Design optimization of shell-and-tube heat exchangers, Appl. Therm. Eng. 28 (2008) 1798–1805, https://doi.org/10.1016/j.applthermaleng.2007.11.009.
[29] R. Khosravi, A. Khosravi, S. Nahavandi, H. Hajabdollahi, Effectiveness of evolutionary algorithms for optimization of heat exchangers, Energy Convers. Manage. 89 (2015) 281–288, https://doi.org/10.1016/j.enconman.2014.09.039.
[30] H. Hajabdollahi, M. Naderi, S. Adimi, A comparative study on the shell and tube and gasket-plate heat exchangers: the economic viewpoint, Appl. Therm. Eng. 92 (2016) 271–282, https://doi.org/10.1016/j.applthermaleng.2015.08.110.
[31] M. Mirzaei, H. Hajabdollahi, H. Fadakar, Multi-objective optimization of shell-and-tube heat exchanger by constructal theory, Appl. Therm. Eng. 125 (2017) 9–19, https://doi.org/10.1016/j.applthermaleng.2017.06.137.
[32] S. Sanaye, H. Hajabdollahi, Multi-objective optimization of shell and tube heat exchangers, Appl. Therm. Eng. 30 (2010) 1937–1945, https://doi.org/10.1016/j.applthermaleng.2010.04.018.
[33] A.V. Azad, M. Amidpour, Economic optimization of shell and tube heat exchanger based on constructal theory, Energy 36 (2011) 1087–1096, https://doi.org/10.1016/j.energy.2010.11.041.
[34] J.M. Ponce-ortega, M. Serna-González, A. Jiménez-gutiérrez, Use of genetic algorithms for the optimal design of shell-and-tube heat exchangers, Appl. Therm. Eng. 29 (2009) 203–209, https://doi.org/10.1016/j.applthermaleng.2007.06.040.
[35] S. Wang, J. Xiao, J. Wang, G. Jian, J. Wen, Z. Zhang, Configuration optimization of shell-and-tube heat exchangers with helical baffles using multi-objective genetic

algorithm based onfluid-structure interaction, Int. Commun. Heat Mass Transf. 85 (2017) 62–69, https://doi.org/10.1016/j.icheatmasstransfer.2017.04.016.
[36] J. Yang, A. Fan, W. Liu, A.M. Jacobi, Optimization of shell-and-tube heat exchangers conforming to TEMA standards with designs motivated by constructal theory, Energy Convers. Manage. 78 (2014) 468–476, https://doi.org/10.1016/j.enconman.2013.11.008.
[37] J. Yang, S. Oh, W. Liu, Optimization of shell-and-tube heat exchangers using a general design approach motivated by constructal theory, Heat Mass Transf. 77 (2014) 1144–1154, https://doi.org/10.1016/j.ijheatmasstransfer.2014.06.046.
[38] S. Fettaka, J. Thibault, Y. Gupta, Design of shell-and-tube heat exchangers using multiobjective optimization, Int. J. Heat Mass Transf. 60 (2013) 343–354, https://doi.org/10.1016/j.ijheatmasstransfer.2012.12.047.
[39] R.V. Rao, A. Saroj, Economic optimization of shell-and-tube heat exchanger using Jaya algorithm with maintenance consideration, Appl. Therm. Eng. 116 (2017) 473–487, https://doi.org/10.1016/j.applthermaleng.2017.01.071.
[40] D.K. Mohanty, Gravitational search algorithm for economic optimization design of a shell and tube heat exchanger, Appl. Therm. Eng. (2016), https://doi.org/10.1016/j.applthermaleng.2016.06.133.
[41] D.K. Mohanty, Application of firefly algorithm for design optimization of a shell and tube heat exchanger from economic point of view, Int. J. Therm. Sci. 102 (2016) 228–238, https://doi.org/10.1016/j.ijthermalsci.2015.12.002.
[42] S.V. Dhavle, A.J. Kulkarni, A. Shastri, I.R. Kale, Design and economic optimization of shell-and-tube heat exchanger using cohort intelligence algorithm, Neural Comput. Appl. (2016), https://doi.org/10.1007/s00521-016-2683-z.
[43] B.V. Babu, S.A. Munawar, Differential evolution strategies for optimal design of shell-and-tube heat exchangers, Chem. Eng. Sci. 62 (2007) 3720–3739, https://doi.org/10.1016/j.ces.2007.03.039.
[44] E.H. de V. Segundo, A.L. Amoroso, V.C. Mariani, L. dos S. Coelho, Economic optimization design for shell-and-tube heat exchangers by a Tsallis differential evolution, Appl. Therm. Eng. 111 (2017) 143–151, https://doi.org/10.1016/j.applthermaleng.2016.09.032.
[45] A. Hadidi, M. Hadidi, A. Nazari, A new design approach for shell-and-tube heat exchangers using imperialist competitive algorithm (ICA) from economic point of view, Energy Convers. Manage. 67 (2013) 66–74, https://doi.org/10.1016/j.enconman.2012.11.017.
[46] T. Kuppan, Heat Exchanger Design Handbook, second ed., Taylor and Francis, Boca Raton, 2013.
[47] R.K. Shah, D.P. Sekulic, Fundamentals of Heat Exchanger Design, John Wiley & Sons, Hoboken, 2003.
[48] R.K. Sinnott, Chemical Engineering Design, fourth ed., Coulson & Richardson's Chemical Engineering, Elsevier, Butterworth-Heinemann, Oxford, 2005.
[49] R.W. Serth, T.G. Lestina, Process Heat Transfer: Principles, Applications and Rules of Thumb, second ed., Elsevier Inc., Oxford, 2014.
[50] X. Yang, Nature-Inspired Metaheuristic Algorithms, second ed., Luniver Press, Frome, 2010.
[51] X.-S. Yang, Mathematical Analysis of Nature-Inspired Algorithms, in: X.-S. Yang (Ed.), Nature-Inspired Algorithms Appl. Optim. Stud. Comput. Intell., Springer International Publishing AG, Cham, 2018, pp. 1–25. https://doi.org/10.1007/978-3-319-67669-2_1.
[52] L. Zhang, L. Liu, X. Yang, Y. Dai, A novel hybrid firefly algorithm for global optimization, PLoS One 11 (2016) 1–17, https://doi.org/10.1371/journal.pone.0163230.
[53] W.A. Khan, N.N. Hamadneh, S.L. Tilahun, J.M.T. Ngnotchouye, A review and comparative study of firefly algorithm and it's modified versions, Optim. Algorithms – Methods Appl., IntechOpen (2016) 281–313, https://doi.org/10.5772/62472.
[54] I. Fister, I. Fister Jr, X. Yang, J. Brest, A comprehensive review of firefly algorithms, Swarm Evol. Comput. 13 (2013) 34–46, https://doi.org/10.1016/j.swevo.2013.06.001.
[55] I. Fister Jr, X. Yang, I. Fister, J. Brest, D. Fister, A brief review of nature-inspired algorithms for optimization, Elektroteh. Vestn. 80 (2013) 1–7.
[56] S.L. Tilahun, J.M.T. Ngnotchouye, Firefly algorithm for discrete optimization problems: a Survey, KSCE J. Civ. Eng. 21 (2017) 535–545, https://doi.org/10.1007/s12205-017-1501-1.
[57] N.D. Kundnaney, D.K. Kushwaha, A critical review on heat exchangers used in oil refinery, in: Afro-Asian Int. Conf. Sci. Eng. Technol., 2015, pp. 1–5.
[58] R. Mukherjee, Effectively design shell-and-tube heat exchangers, Chem. Eng. Prog. (1998).
[59] M. Zhang, F. Meng, Z. Geng, CFD simulation on shell-and-tube heat exchangers with small-angle helical baf fl es, Front. Chem. Sci. Eng. (2015) 1–11, https://doi.org/10.1007/s11705-015-1510-x.
[60] M. Bahiraei, S.M. Naghibzadeh, M. Jamshidmofid, Efficacy of an eco-friendly nanofluid in a miniature heat exchanger regarding to arrangement of silver nanoparticles, Energy Convers. Manage. 144 (2017) 224–234, https://doi.org/10.1016/j.enconman.2017.04.076.
[61] A.D. Kraus, Heat Exchangers, in: A. Bejan, A.D. Kraus (Eds.), Heat Transf. Handb., John Wiley & Sons, Hoboken, 2003, pp. 797–911.
[62] J. Taborek, Shell-and-tube heat exchangers: single-phase flow, in: E.U. Schlunder (Ed.), Heat Exch. Des. Handb., Hemisphere Publishing Corporation, New York, 1983, pp. 982–1058.
[63] M.R. Meas, T. Bello-Ochende, Thermodynamic design optimisation of an open air recuperative twin-shaft solar thermal Brayton cycle with combined or exclusive reheating and intercooling, Energy Convers. Manage. 148 (2017) 770–784, https://doi.org/10.1016/j.enconman.2017.06.043.
[64] R.T. Ogulata, F. Doba, Experiments and entropy generation minimization analysis of a cross-flow heat exchanger, Int. J. Heat Mass Transf. 41 (1998) 373–381.
[65] T.R. Ogulata, F. Doba, T. Yilmaz, Irreversibility analysis of cross ¯ ow heat exchangers, Energy Convers. Manage. 41 (2000) 1585–1599.
[66] Z. Zhang, C. Jiang, Y. Zhang, W. Zhou, B. Bai, Virtual entropy generation (VEG) method in experiment reliability control: Implications for heat exchanger measurement, Appl. Therm. Eng. 110 (2017) 1476–1482, https://doi.org/10.1016/j.applthermaleng.2016.09.051.
[67] K.M. Koorts, Minimisation and Structural Design for Industrial Heat Exchanger Optimisation, M.Sc. Thesis, Department of Mechanical and Aeronautical Engineering, University of Pretoria, 2014.
[68] G. Lorenzini, E.X. Barreto, C.C. Beckel, P.S. Schneider, L.A. Isoldi, E.D. Dos Santos, L.A.O. Rocha, Constructal design of I-shaped high conductive pathway for cooling a heat-generating medium considering the thermal contact resistance, Int. J. Heat Mass Transf. 93 (2016) 770–777, https://doi.org/10.1016/j.ijheatmasstransfer.2015.10.015.
[69] A.H. Reis, Constructal theory: from engineering to physics, and how flow systems develop shape and structure, Appl. Mech. Rev. 59 (2006) 269, https://doi.org/10.1115/1.2204075.
[70] Aalco, Stainless steel tubular products, Aalco Met. Ltd., 2015, pp. 1–18.
[71] X. Yang, Nature-Inspired Optimization Algorithms, first ed., Elsevier Inc., London, 2014.